ACS APPLIED ENERGY MATERIALS

www.acsaem.org Article

Enhancing Thermoelectric Performance of NaCdSb-Based Materials Through Isovalent Substitution

Minglong Wang, Honghao Yao, Kejia Liu, Yu-Jun Zhao,* and Yue Chen*

Cite This: ACS Appl. Energy Mater. 2025, 8, 11741−11748 Read Online

ACCESS | Metrics & More | Article Recommendations | Supporting Information

ABSTRACT: Thermoelectric materials, which enable the direct conversion of heat into electricity and vice versa, are critical for sustainable energy solutions. Recently, the Zintl-phase compound NaCdSb was discovered to have a zT value of 1.3 at 673 K in its pristine form. Subsequently, its zT value was increased to 1.41 through carrier concentration tuning, but optimization remains limited due to experimental constraints. In this study, we employ first-principles calculations to systematically investigate the thermoelectric properties of NaCdSb-based materials. By optimizing carrier concentration, the predicted power factor of NaCdSb can be significantly enhanced. Furthermore, isovalent substitution with Li and K decouples the interdependence of thermoelectric parameters. K alloying improves band convergence, boosting the Seebeck coefficient and enhancing the power factor across a large carrier concentration range. Considering the impact of heavy-element alloying on lattice thermal conductivity and given that the electronic thermal conductivity of KNCS remains almost unchanged, the zT of KNCS is also expected to increase. Our work demonstrates that K alloying can be an effective strategy to enhance the thermoelectric performance of NaCdSb-based materials, making them potential candidates for high-efficiency TE applications.

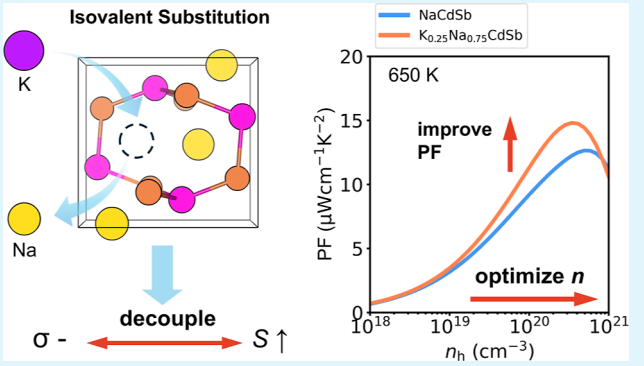

KEYWORDS: *NaCdSb, Zintl phase, thermoelectric, isovalent substitution, band convergence, first-principles calculation, alloy*

INTRODUCTION

Thermoelectric (TE) materials, a type of semiconductor, enable the direct conversion of heat into electricity and vice versa, providing sustainable solutions for waste heat recovery, temperature control, and other applications.[1−4] The performance of TE materials is quantified by the thermoelectric figure of merit zT, which is calculated using the formula $zT = \sigma S^2 T/(\kappa_e + \kappa_L)$. Here, S represents the Seebeck coefficient, σ denotes electrical conductivity, κ_e is the electronic thermal conductivity, and κ_L is the lattice thermal conductivity. The term σS^2 is known as the power factor (PF), a key parameter for evaluating electrical transport properties. Generally, optimal TE performance requires a high power factor and low thermal conductivity. However, due to the complex and often inversely related interdependencies among the various transport properties, the development of efficient TE materials remains challenging.[5,6]

Recently, Guo et al. proposed a new 1−1−1 type Zintl compound, NaCdSb, which achieved a high zT value of 1.3 at 673 K without any optimization.[7] Liu et al. improved the carrier concentration through sodium deficiency and silver doping, optimizing the thermoelectric performance and achieving a zT value of 1.41 at 673 K.[8] As a Zintl phase, NaCdSb is a unique polar intermetallic compound exhibiting both ionic and covalent bonding.[9,10] Due to this dual bonding nature, Zhang et al. demonstrated that Na^+ ions exhibit rattling-like dissipation properties at high temperatures from first-principles calculations, contributing to its low lattice thermal conductivity.[11] This aligns with the "phonon-glass, electron-crystal" (PGEC) concept, making NaCdSb-based materials promising for thermoelectric applications.[12,13] Further research and optimization in NaCdSb-based materials are therefore highly warranted.

To further optimize the thermoelectric properties of Zintl phases, various strategies have been employed over the past decade, including band engineering,[14−18] defect engineering,[19−21] entropy engineering,[22,23] and structural manipulation.[24] Among these, isovalent substitution emerges as a potentially effective method. This approach can mitigate the interdependence of thermoelectric properties by promoting band convergence, thus enabling the independent optimization of these properties.[25,26]

Received: June 23, 2025
Revised: July 19, 2025
Accepted: July 24, 2025
Published: July 29, 2025

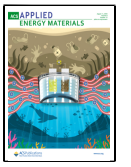

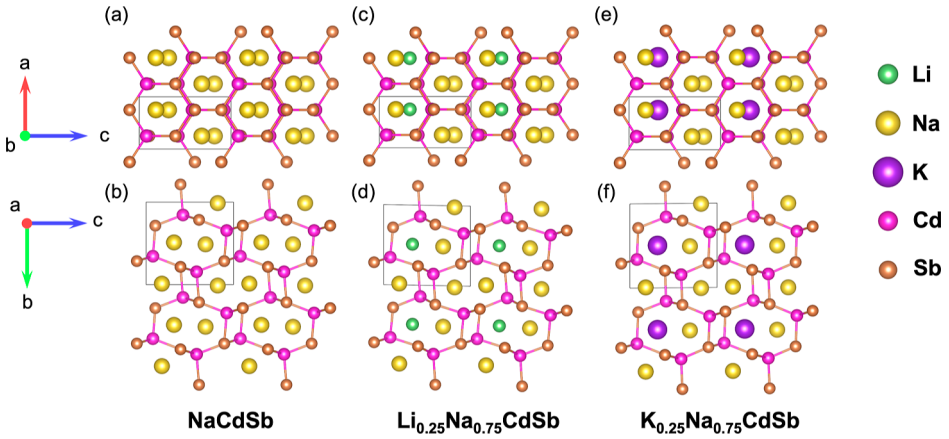

Figure 1. Crystal structure of (a,b) NaCdSb, (c,d) $Li_{0.25}Na_{0.75}CdSb$ and (e,f) $K_{0.25}Na_{0.75}CdSb$.

In this article, we systematically investigate the thermoelectric properties of the Zintl-phase compound NaCdSb and its Li/K-alloyed derivatives. Through computational simulation, we explore the effects of isovalent substitution on the electronic structure and transport properties of these materials. Our results reveal that optimizing carrier concentration and introducing heavier elements like potassium can significantly enhance the power factor and decouple the interdependence of thermoelectric parameters, thereby improving overall performance. This study provides valuable insights into the potential of NaCdSb-based alloys as high-performance thermoelectric materials.

COMPUTATIONAL DETAILS

The calculations are performed in the framework of Density Functional Theory (DFT) as implemented in the Vienna ab initio Simulation Package (VASP).[27,28] The revised PBE for solids (PBEsol) in Generalized Gradient Approximation (GGA) was set to describe the exchange−correlation energy.[29] The plane-wave cutoff was chosen to be 500 eV. A Γ-centered *k*-point grid with a *k*-spacing of 0.05 2π/Å was used for structural relaxations, the convergence criteria for the total energy and ionic forces were set to 10^{-5} eV and 0.01 eV/Å, respectively. In the self-consistent field (SCF) calculations, as well as in the computations of band structures and density of states (DOS), we reduce the *k*-spacing to 0.03 2π/Å, and use 10^{-8} eV for the convergence criterion. Given that the PBE series functional tends to underestimate band gaps, which significantly influence electrical transport properties, we have opted for the modified Becke-Johnson (mBJ) potential to obtain more precise band gap values.[30] To cross-validate the reliability of the mBJ method, the Heyd−Scuseria−Ernzerhof (HSE06) hybrid functional was also employed.[31] Based on first-principles data, we utilized the ab initio scattering and transport (AMSET) package to compute electrical transport properties from acoustic deformation potential (ADP), ionized impurity scattering (IMP), and polar optical phonon (POP) scattering.[32,33]

RESULTS

NaCdSb-Based Alloys. Savelsberg and Schäfer first determined the crystal structure of NaCdSb (NCS), characterized by an orthorhombic structure with the *Pnma* space group.[34] Recently, Guo et al. successfully synthesized NaCdSb, with a minor impurity phase of Na_2O_2 present. Without any doping optimization or structural modification, NaCdSb achieved a high power factor of 11.56 μW cm^{-1} K^{-2} and a maximum zT of 1.3 at 673 K, indicating significant potential for performance enhancement.[7] Furthermore, Liu et al. synthesized $Na_{0.99}Cd_{0.995}Ag_{0.005}Sb$ by Ag doping and introducing a small amount of Na deficiency. This approach improved the power factor while maintaining a low lattice thermal conductivity, resulting in a higher zT of 1.41 at 673 K. Additionally, it enhanced the performance at lower temperatures, achieving an average zT value of 0.81 over the temperature range of 300−673 K.[8]

As a Zintl phase material, NCS comprises Na^+ cations and an anionic framework formed by Cd and Sb atoms. As shown in Figure 1a,b, the Cd and Sb atoms form puckered pseudohexagonal two-dimensional layers interconnected by zigzag ladders and four-membered rings. Each cage-like structure created by the Cd−Sb framework houses two Na^+ cations at its center. As Na^+ cations do not form stable covalent bonds with the Cd−Sb framework, they exhibit rattling-like dissipation at high temperatures, contributing to the low lattice thermal conductivity.[11] Meanwhile, NaCdSb demonstrates good electrical conductivity[7,8] due to the covalent bond network formed by Cd−Sb. These characteristics align NaCdSb-based materials with the PGEC concept.[12,13] The coexistence of ionic and covalent bonds within its structure aligns with the PGEC concept, positioning it as a promising candidate for thermoelectric applications.[12,13]

Although experimental and theoretical studies have identified NCS as a promising thermoelectric material, further systematic research is essential for optimizing its performance.[7,8,35] Isovalent substitution, which involves replacing a host atom with an impurity atom of the same valence, was shown to decouple the interdependence of thermoelectric properties, by promoting band convergence, thus enabling the independent optimization of these properties.[25,26] For instance, replacing Te with Se in Bi_2Te_3 based materials via isovalent substitution decreases electrical conductivity while simultaneously enhancing the Seebeck coefficient and power factor.[36−38] Consequently, we employ isovalent substitution with Li and K for Na. As shown in Figure 1c−f, we introduce either Li or K to replace one Na in the primitive cell, which contains four Na atoms, yielding the alloys $Li_{0.25}Na_{0.75}CdSb$ (LNCS) and $K_{0.25}Na_{0.75}CdSb$ (KNCS).

To achieve a more precise calculation of the lattice constants in alignment with experimental values, we utilized the PBEsol

https://doi.org/10.1021/acsaem.5c01933
ACS Appl. Energy Mater. 2025, 8, 11741−11748

functional to describe the exchange−correlation energy.[29] As presented in Table 1, the calculated lattice constants for

Table 1. Crystallographic Data of NaCdSb and Its Alloies Calculated Using Different Functionals[a]

	functional	a (Å)	b (Å)	c (Å)	V (Å^3)
NaCdSb (Guo et al.[7])	experiment	4.73	7.99	8.47	319.59
NaCdSb	PBE	4.84	8.06	8.61	336.13
	PBEsol	4.78	7.93	8.40	318.54
$Li_{0.25}Na_{0.75}CdSb$	PBEsol	4.71	7.78	8.43	309.00
$K_{0.25}Na_{0.75}CdSb$	PBEsol	4.85	8.09	8.38	328.79

[a]The lattice constants obtained by Guo et al. from experiments are also included fro comparison.

NaCdSb are in agreement with experimental data. Following alloying, the smaller size Li results in a reduction of the unit cell volume, while the larger size K leads to an increase in the unit cell volume. Additionally, both structures exhibit more pronounced changes in the a and b axes.

Electronic Structures. The commonly employed PBE functional in DFT calculations tends to underestimate the band gap.[39] Previous studies have utilized the Heyd−Scuseria−Ernzerhof (HSE06) hybrid functional for the calculations, yielding a band gap of approximately 0.5 eV.[7,35,40] However, the computational demand of HSE06 is considerably high, which prompts the exploration of alternative methods. In this work, we have employed mBJ potential, which has been reliably applied in other thermoelectric materials, to correct the band gaps.[30] As shown in Table 2, the band gap

Table 2. Band Gap E_g of NaCdSb and Its Alloies Calculated from Different Functionals

	functional	E_g (eV)
NaCdSb[7]	PBE + HSE06	0.50
NaCdSb[11]	PBE + HSE06	0.45
NaCdSb	PBE + HSE06	0.44
	PBEsol + HSE06	0.61
	PBEsol + mBJ	0.75
$Li_{0.25}Na_{0.75}CdSb$	PBEsol + mBJ	0.64
$K_{0.25}Na_{0.75}CdSb$	PBEsol + mBJ	0.82

obtained from PBEsol + HSE06 is slightly larger than that from PBE + HSE06, and the result from PBEsol + mBJ is even larger. This indicates that PBEsol tends to increase the band gap, as does mBJ compared to HSE06. Figure S1 in the Supporting Information compares the band structures obtained from mBJ and HSE06, revealing their overall similarity.

In Figure 2, the valence band maximum (VBM) is set to zero for a clearer comparison of the band structures among the three different systems. It is observed that in NCS, both VBM and the conduction band minimum (CBM) exhibit band convergence, a feature that has been eloquently described in previous works, indicating a highly favorable band structure of thermoelectric.[7,35] The higher degeneracy of VBM, with three bands in close proximity, is also reflected in the density of states (DOS), suggesting potentially superior Seebeck coefficients for the p-type systems. Although CBM has a lower band degeneracy, their lighter shape implies that the electrical conductivity for the n-type systems may be higher than that for the p-type.

As shown in Figure 2b−d, the band structures and DOS of LNCS and KNCS are similar to those of NCS. Therefore, similar to the analysis of NCS, the electrical conductivity of n-type systems is expected to be superior to that of p-type, while the Seebeck coefficient of p-type systems would be superior to that of n-type. Comparing the band structures, LNCS shows valence band convergence close to that of NCS, while the conduction band of NCS is more converged. In contrast, KNCS exhibits the most pronounced band convergence in both the conduction and valence bands. As shown in Figure 2d, this characteristic results in a higher DOS around the VBM for KNCS compared to the other two systems. This suggests that p-type KNCS may possess a larger Seebeck coefficient.

Transport Properties. Given that the carrier concentration may increase due to intrinsic excitation of electrons, the carrier concentration n we use in calculation is consistent with experimental data,[7] as indicated by the red line in Figure 3a. While calculating mobility using the constant relaxation time approximation is convenient, this approach requires arbitrarily selecting a value for the relaxation time and does not reflect the impact of energy and temperature on the relaxation time. By employing ADP, IMP and POP, as shown in Figure 3b, the relaxation time varies with the carrier concentration and temperature, which enhances the accuracy of the computational results.[32]

Figure 3c,d display a comparison between our calculated electrical conductivity and Seebeck coefficient with the experimental results. Observing the orange line, which denotes the experimental results, we note that the electrical conductivity exhibits a decrease before an increase at 373 K. The initial decline in electrical conductivity is due to the weak intrinsic excitation of carriers at low temperatures, along with a reduction in carrier mobility as the temperature rises. Above 373 K, the carrier concentration increases sharply because of stronger intrinsic excitation, which in turn causes the electrical conductivity to rise. The Seebeck coefficient shows an inverse relationship with temperature, peaking at 423 K before it starts to decrease. The trends of the calculated electrical conductivity and Seebeck coefficient are in good agreement with the experimental data, although there is a difference in their absolute values.

The discrepancy between the calculated results and experimental data stems from several factors. First, our method is based on the rigid band assumption, which does not account for the effects of temperature and doping on the band structure.[41] Second, the core state level method used in the AMSET package is sensitive to volume deformations. This sensitivity can lead to an overestimation of the deformation potential constant, resulting in an underestimation of relaxation times and electrical conductivity-related quantities.[32,42−44] Third, our analysis considers only the primary scattering mechanisms, whereas other scattering mechanisms may be at play during charge transport. Despite these discrepancies, the overall trends of the parameters align well with experimental values. Given that our study focuses on comparing the performance changes among the three systems, we believe the conclusions drawn from the current methodology are qualitatively reliable.

To facilitate a more in-depth and systematic analysis, we calculated the impact of various carrier concentration and temperatures, as well as different types of carriers on performance. As shown in Figure 4, the color code represents

https://doi.org/10.1021/acsaem.5c01933
ACS Appl. Energy Mater. 2025, 8, 11741−11748

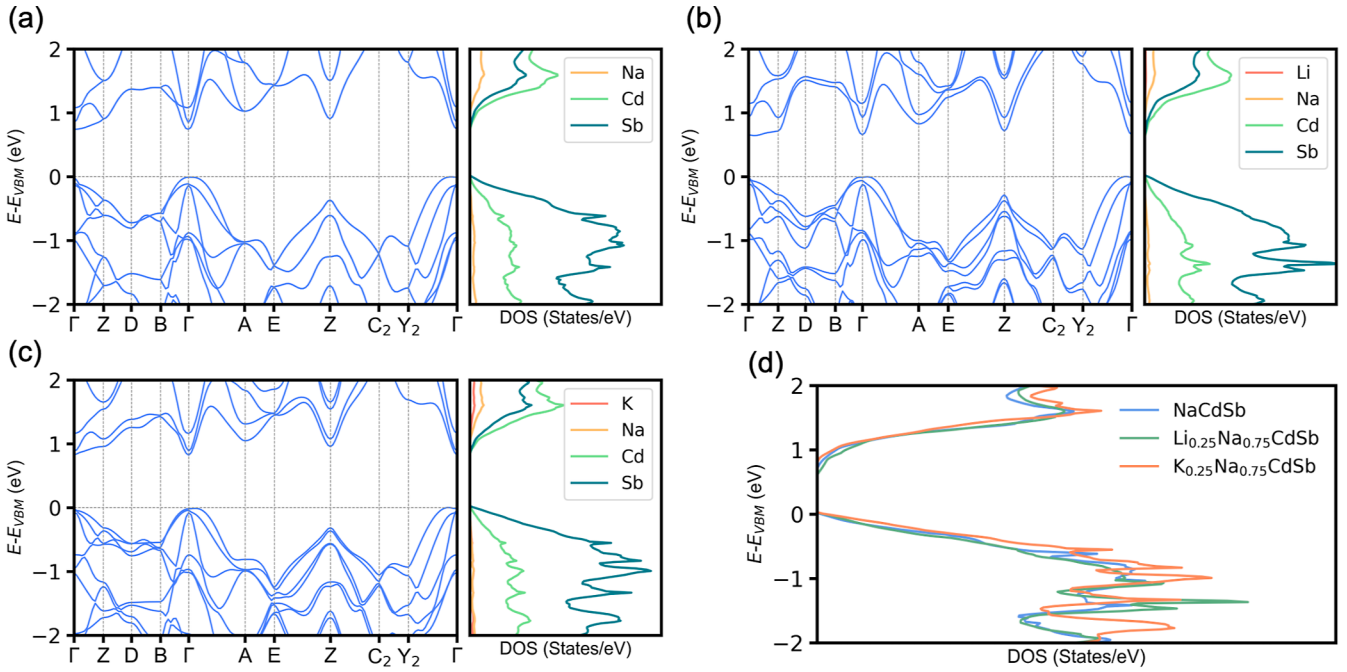

Figure 2. Band structures and projected DOS of (a) NaCdSb, (b) $Li_{0.25}Na_{0.75}CdSb$ and (c) $K_{0.25}Na_{0.75}CdSb$. (d) Total DOS of the three systems.

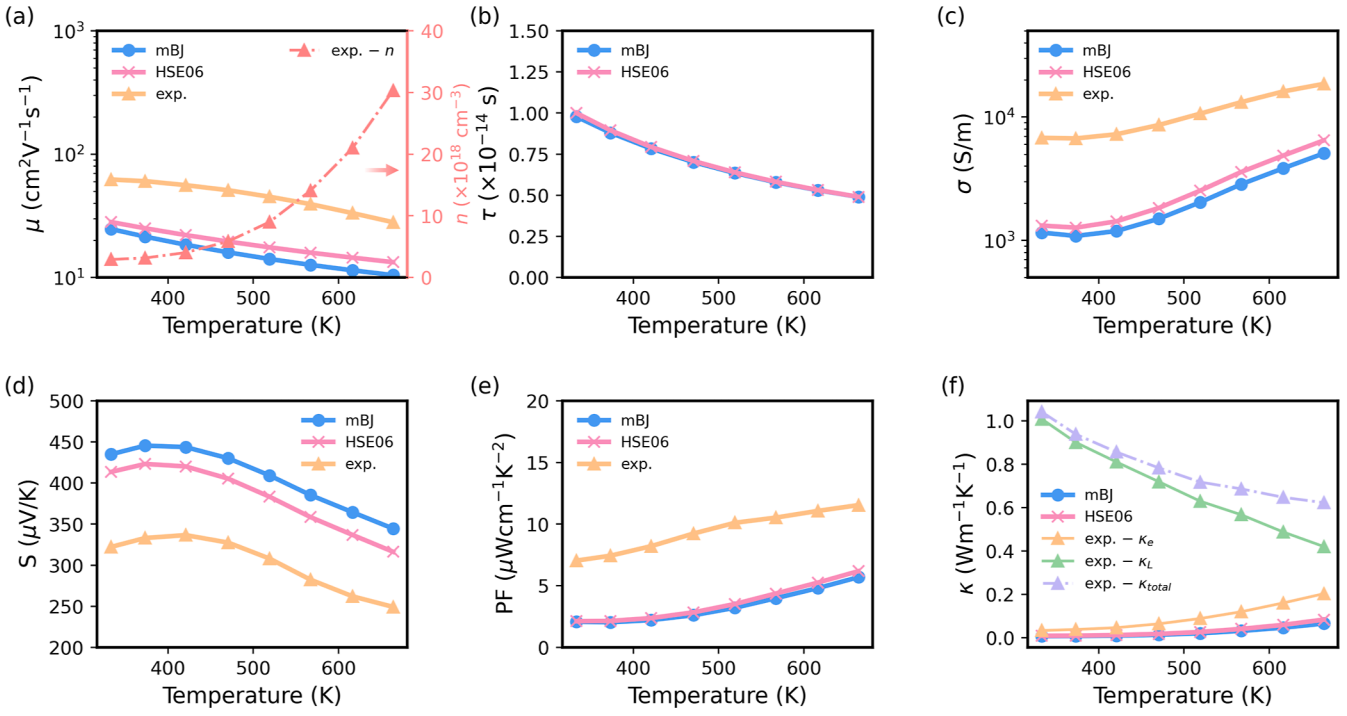

Figure 3. (a) Mobility, (b) relaxation time, (c) electrical conductivity, (d) Seebeck coefficient, (e) power factor, and (f) thermal conductivity of NaCdSb as functions of temperature. The experimental carrier concentration[7] at different temperatures shown in panel (a) have been taken in our calculations. The calculations were performed using AMSET,[32] taking into account ADP, IMP and POP.

the magnitude of the power factor, with the deepest red indicating the highest power factor.

An increase in carrier concentration leads to a higher electrical conductivity but a decrease in the Seebeck coefficient, thus there exists an optimal carrier concentration for maximizing the PF. As depicted in Figure 4a–c, the trends of PF variation with temperature and carrier concentration for these three p-type NCS-based alloys are similar, with the maximum PF occurring near a carrier concentration of 3 × 10^{20} cm^{-3}. Clearly, the maximum PF of KNCS is significantly higher than those of the other two systems. Figure 4d–f display the PF variation for the three systems in their n-type systems. Similar to what was observed in the p-type, the performance of n-type KNCS is significantly higher than that of n-type LNCS and NCS. The best performance is observed at a carrier concentration near 3 × 10^{19} cm^{-3}, which is relatively low compared to the p-type. Given that the performance of the three systems in their p-type configuration

https://doi.org/10.1021/acsaem.5c01933
ACS Appl. Energy Mater. 2025, 8, 11741−11748

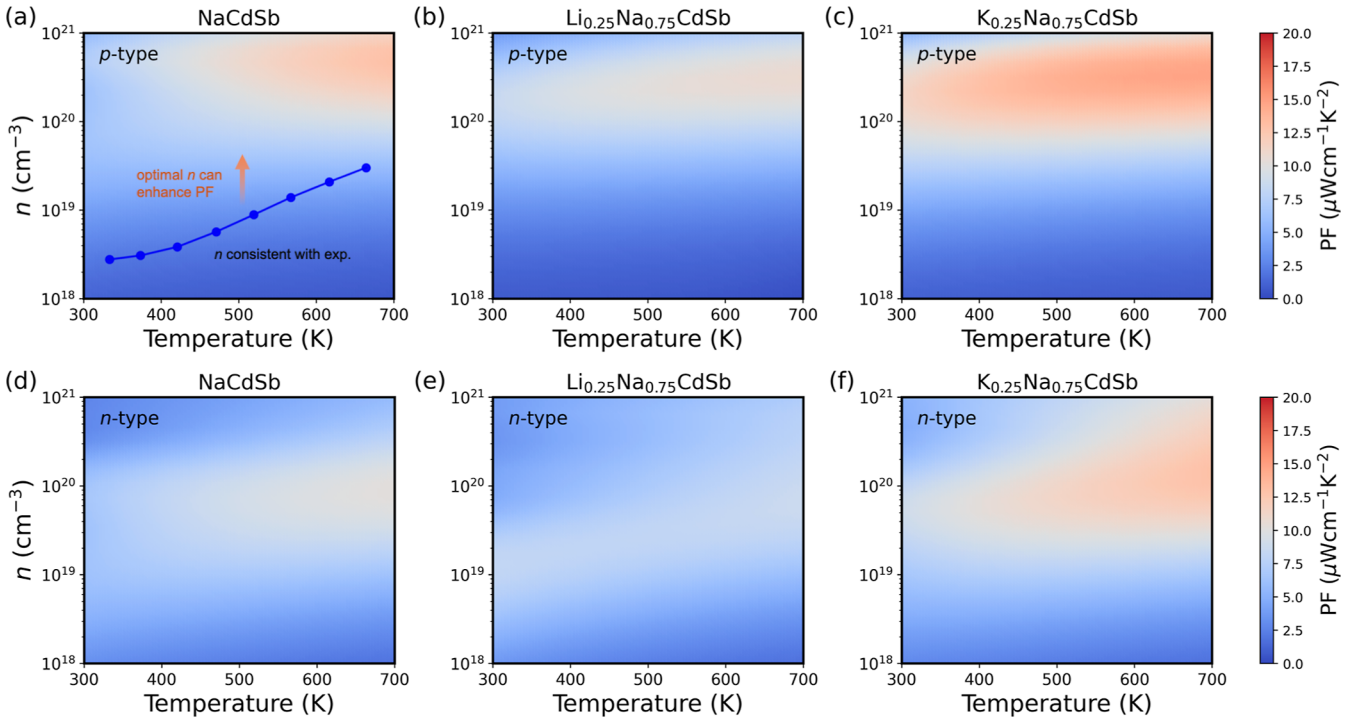

Figure 4. Power factor as a function of temperature and carrier concentration for p-type and n-type (a,d) NaCdSb, (b,e) $Li_{0.25}Na_{0.75}CdSb$, and (c,f) $K_{0.25}Na_{0.75}CdSb$. The color intensity represents the magnitude of power factor. The blue line in (a) indicates the variation of carrier concentration as observed experimentally in ref 7.

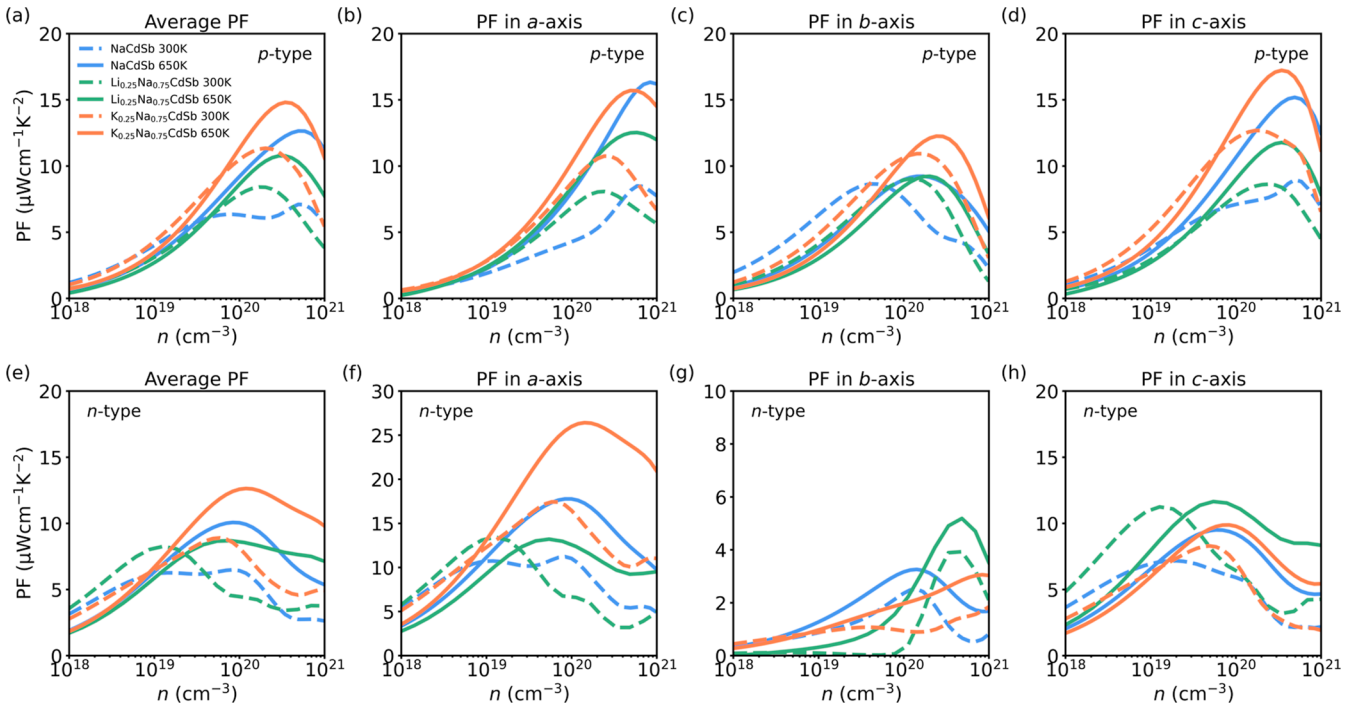

Figure 5. Power factors for p-type (a−d) and n-type (e−h) NaCdSb, $Li_{0.25}Na_{0.75}CdSb$ and $K_{0.25}Na_{0.75}CdSb$ as a function of carrier concentration at 300 and 650 K.

is superior to their n-type, and considering that the experimental samples of NCS are also natively p-type, it is expected that p-type doping holds greater potential for NCS-based alloys. We also find that the introduction of K significantly enhances the PF, and thus we will conduct a more detailed analysis to discuss how K influences the performance.

Figure 5 illustrates the variation of PF with carrier concentration, which allows for a more intuitive comparison of the performance among these three systems. Experimental results confirm that NCS remains stable up to 673 K.[7,8] Therefore, we have selected 300 and 650 K to represent the performance at low and high temperatures, respectively.

https://doi.org/10.1021/acsaem.5c01933
ACS Appl. Energy Mater. 2025, 8, 11741−11748

In Figure 5a, it is evident that the maximum PF for each system at high temperatures is greater than that at low temperatures for the p-type materials. Consequently, we will focus on the performance changes of each system at high temperatures within the p-type context. As observed in Figure 4, the PF increases with the rise in carrier concentration, but the intrinsic carrier concentration in experiments at high temperatures is only 3×10^{19} cm^{-3}. By optimizing the carrier concentration, the PF of NCS may be improved significantly. NCS, LNCS, and KNCS reach their peak PFs at a carrier concentration of about 2×10^{20} cm^{-3}. Notably, KNCS significantly outperforms the other two systems at both high and low temperatures across all carrier concentrations. To explore the properties of single crystal, in Figure 5b–d, we compare the variations in PF across different directions. A common feature among the three systems is that performance is highest along the *c*-axis. Furthermore, the optimal PF along the *b*-axis is associated with the lowest carrier concentration. This may be attributed to the differences in carrier effective mass along various directions, a factor that will be analyzed in greater detail later.

Figure 5e shows the results for n-type NCS, LNCS, and KNCS. It is seen that the optimal carrier concentration corresponding to the maximum PF is 3×10^{19} cm^{-3}, which is lower than that for the p-type. Additionally, the peak PF values are lower compared to the p-type systems.

Furthermore, when examining the performance across the three principal axes in Figure 5f–h, it is evident that the performance along the *b*-axis is lower than that along the *a* and *c*-axis. The PF of the n-type along the *b*-axis is significantly lower than that along the *a* and *c*-axis, demonstrating strong anisotropy. This may be attributed to the differences in carrier effective mass across various directions. Taking the band structure of NaCdSb as an example, the directions $Y_2 \rightarrow \Gamma$, $\Gamma \rightarrow Z$, and $\Gamma \rightarrow B$ correspond to the *a*, *b*, and *c*-axis, respectively. As shown in Figure 2a, the CBM along the *b*-axis is a heavier band, indicating a larger carrier effective mass compared to the other two directions. This leads to the average PF of the n-type being less favorable than that of the p-type. Additionally, KNCS exhibits a higher PF along the *a*-axis compared to the *c*-axis, while the differences between the *a*-axis and *c*-axis are less pronounced for NCS and LNCS. Despite the average PF of the n-type being lower than that of the p-type, the n-type PF along the *a*-axis is the most superior.

Next, we conduct a more detailed analysis combining band structure, electrical conductivity, Seebeck coefficient, and electronic thermal conductivity to understand how the introduction of K enhances the performance of NCS and the origins of performance differences between the n-type and p-type. From Figures S2 and S3 in the Supporting Information, we observe that the differences in electrical conductivity between KNCS and NCS are minor. Furthermore, isovalent substitution increases the band degeneracy in KNCS. This enhances the DOS while maintaining the carrier effective mass, thereby decoupling the interdependence of these parameters. As a result, the power factors in both n-type and p-type materials are improved by increasing the Seebeck coefficients while preserving electrical conductivities. Comparing to the conduction bands, the valence bands are heavier. Hence, the lower scattering rates and higher mobility of the n-type carriers result in a higher electrical conductivity. On the other hand, due to the large electronic DOS near the VBM, the p-type Seebeck coefficient is superior to the n-type, resulting in a higher p-type power factor.

The thermoelectric efficiency of a material, quantified by the figure of merit zT, depends critically on its thermal conductivity. The total thermal conductivity consists of lattice thermal conductivity and electronic thermal conductivity, $\kappa = \kappa_L + \kappa_e$. In pristine NCS, the lattice thermal conductivity dominates the total thermal conductivity due to its intrinsically low carrier concentration, as shown in Figure 3f. When heavier K atoms are doped into the NCS-based materials, the phonon dispersion undergoes significant modification. This alteration enhances phonon scattering rates, leading to a reduction in lattice thermal conductivity for KNCS compared to NCS.[45,46] Figures S4 and S5 in the Supporting Information show that KNCS has similar electronic thermal conductivity to NCS, thus the total thermal conductivity of KNCS is expected to be lower than that of NCS suggesting that KNCS is also likely to achieve a higher zT.

CONCLUSION

In summary, we have systematically investigated the thermoelectric behavior of the Zintl-phase NaCdSb and its Li/K-alloyed derivatives. Our results demonstrate that optimizing carrier concentration significantly enhances the power factor of NCS and its alloys, with p-type systems outperforming the n-type counterparts. Introducing K elevates the PF, achieving significantly improvements for the p-type and n-type systems at 650 K, respectively. Through analysis of the band structure and related thermoelectric parameters, we demonstrate that substituting heavier K atoms for Na enhances band degeneracy. This improves the Seebeck coefficient and power factor, while electrical conductivity remains less affected. Additionally, KNCS is expected to have a lower thermal conductivity than NCS, suggesting KNCS is likely to achieve a higher zT. This mechanism effectively decouples the interdependence of thermoelectric parameters, highlighting the unique advantages of K alloying.

ASSOCIATED CONTENT

Supporting Information

The Supporting Information is available free of charge at https://pubs.acs.org/doi/10.1021/acsaem.5c01933.

Band structures of pristine NaCdSb calculated using mBJ and HSE06 functionals. Detailed electrical and thermal transport properties of p-type and n-type NaCdSb-based alloys (K- and Li-substituted systems), including electrical conductivity, Seebeck coefficient, and electronic thermal conductivity (PDF)

AUTHOR INFORMATION

Corresponding Authors

Yu-Jun Zhao − *Department of Physics, South China University of Technology, Guangzhou 510640, China;* orcid.org/0000-0002-6923-1099; Email: zhaoyj@scut.edu.cn

Yue Chen − *Department of Mechanical Engineering, The University of Hong Kong, Hong Kong SAR, China;* Email: yuechen@hku.hk

Authors

Minglong Wang − *Department of Physics, South China University of Technology, Guangzhou 510640, China; Department of Mechanical Engineering, The University of*

https://doi.org/10.1021/acsaem.5c01933
ACS Appl. Energy Mater. 2025, 8, 11741−11748

Hong Kong, Hong Kong SAR, China; orcid.org/0009-0008-6627-158X

Honghao Yao − *Department of Mechanical Engineering, The University of Hong Kong, Hong Kong SAR, China;* orcid.org/0000-0003-3344-5447

Kejia Liu − *Department of Mechanical Engineering, The University of Hong Kong, Hong Kong SAR, China*

Complete contact information is available at: https://pubs.acs.org/10.1021/acsaem.5c01933

Notes

The authors declare no competing financial interest.

■ ACKNOWLEDGMENTS

This work is financially supported by Guangdong Major Project of Basic and Applied Basic Research (2020B0301030001), the Research Grants Council of Hong Kong (C7002-22Y, 17318122, and C6020-22GF), and National Natural Science Foundation of China (12474229). The authors are grateful for the research computing facilities offered by ITS, HKU, and the high performance computational center at SCUT.

■ REFERENCES

(1) Goldsmid, H. J. *Thermoelectric Refrigeration*; Springer US: Boston, MA, 1964.

(2) Bell, L. E. Cooling, Heating, Generating Power, and Recovering Waste Heat with Thermoelectric Systems. *Science* **2008**, *321*, 1457−1461.

(3) Poudel, B.; Hao, Q.; Ma, Y.; Lan, Y.; Minnich, A.; Yu, B.; Yan, X.; Wang, D.; Muto, A.; Vashaee, D.; Chen, X.; Liu, J.; Dresselhaus, M. S.; Chen, G.; Ren, Z. High-Thermoelectric Performance of Nanostructured Bismuth Antimony Telluride Bulk Alloys. *Science* **2008**, *320*, 634−638.

(4) LeBlanc, S. Thermoelectric generators: Linking material properties and systems engineering for waste heat recovery applications. *Sustain. Mater. Technol.* **2014**, *1*−*2*, 26−35.

(5) *Electron Transport in Compound Semiconductors*; Nag, B., Cardona, M., Fulde, P., Queisser, H.-J., Eds.; Springer: Berlin Heidelberg, 1980; Vol. *11*.

(6) Scheidemantel, T. J.; Ambrosch-Draxl, C.; Thonhauser, T.; Badding, J. V.; Sofo, J. O. Transport coefficients from first-principles calculations. *Phys. Rev. B* **2003**, *68*, 125210.

(7) Guo, K.; Zhang, Y.; Yuan, S.; Tang, Q.; Lin, C.; Luo, P.; Yang, J.; Pan, S.; Zhao, L.-D.; Cheng, G.; Zhang, J.; Luo, J. NaCdSb: An Orthorhombic Zintl Phase with Exceptional Intrinsic Thermoelectric Performance. *Angew. Chem., Int. Ed.* **2023**, *62*, No. e202212515.

(8) Liu, K.; Chen, C.; Cheng, J.; Ma, X.; Li, J.; Bao, X.; Li, H.; Zhang, Q.; Chen, Y. Realizing a High Thermoelectric Conversion Efficiency in Zintl-phase NaCdSb via Suppressing the Intrinsic Carrier Excitation. *Adv. Funct. Mater.* **2025**, *35*, 2419145.

(9) Nesper, R. Bonding Patterns in Intermetallic Compounds. *Angew. Chem., Int. Ed. Engl.* **1991**, *30*, 789−817.

(10) Nesper, R. The Zintl-Klemm Concept − A Historical Survey. *Z. Anorg. Allg. Chem.* **2014**, *640*, 2639−2648.

(11) Zhang, P.; Tang, S.; Wan, D.; Li, X.; Ai, P.; Guo, W.; Yan, T.; Zhang, Y.; Li, Q.; Bai, S. Cation-Driven Vibrational Hierarchy in NaCdX (X = As, Sb) Thermoelectrics: From Static Insulation to Rattling-Like Dissipation. *Chem. Mater.* **2025**, *37*, 1891−1905.

(12) Kauzlarich, S. M.; Brown, S. R.; Jeffrey Snyder, G. Zintl phases for thermoelectric devices. *Dalton Trans.* **2007**, 2099−2107.

(13) Toberer, E. S.; May, A. F.; Snyder, G. J. Zintl Chemistry for Designing High Efficiency Thermoelectric Materials. *Chem. Mater.* **2010**, *22*, 624−634.

(14) Guo, M.; Zhai, W.; Li, J.; Zhu, J.; Guo, F.; Liu, Z.; Liu, M.; Zhu, Y.; Dong, X.; Zhang, Y.; Zhang, Q.; Cai, W.; Sui, J. High Thermoelectric Performance of $CaMg_2$ Bi_2 Enabled by Dynamic Doping and Orbital Alignment. *Adv. Funct. Mater.* **2022**, *32*, 2200407.

(15) Shi, X.; Song, S.; Gao, G.; Ren, Z. Global band convergence design for high-performance thermoelectric power generation in Zintls. *Science* **2024**, *384*, 757−762.

(16) Askarpour, V.; Maassen, J. First-principles analysis of intravalley and intervalley electron-phonon scattering in thermoelectric materials. *Phys. Rev. B* **2023**, *107*, 045203.

(17) Zhang, Z.; Yao, H.; Jia, X.; Wang, X.; Li, X.; Chen, C.; Lin, X.; Sui, J.; Liu, X.; Mao, J.; Xie, G.; Zhang, Q. Band convergence and phonon engineering to optimize the thermoelectric performance of CaCd2Sb2. *Appl. Phys. Lett.* **2022**, *120*, 041901.

(18) Wang, N.; Li, M.; Xiao, H.; Gao, Z.; Liu, Z.; Zu, X.; Li, S.; Qiao, L. Band degeneracy enhanced thermoelectric performance in layered oxyselenides by first-principles calculations. *npj Comput. Mater.* **2021**, *7*, 18.

(19) Zhang, Z.; Wang, X.; Liu, Y.; Chen, C.; Yao, H.; Yin, L.; Li, X.; Li, S.; Zhang, F.; Bai, F.; Sui, J.; Yu, B.; Cao, F.; Liu, X.; Mao, J.; Xie, G.; Zhang, Q. Balancing the anionic framework polarity for enhanced thermoelectric performance in YbMg2Sb2 Zintl compounds. *J. Materiomics* **2019**, *5*, 583−589.

(20) Yang, C.; Guo, K.; Yang, X.; Xing, J.; Wang, K.; Luo, J.; Zhao, J.-T. Realizing High Thermoelectric Performance in BaCu2−xAgxTe2 through Enhanced Carrier Effective Mass and Point-Defect Scattering. *ACS Appl. Energy Mater.* **2019**, *2*, 889−895.

(21) Wu, L.; Zhou, Z.; Han, G.; Zhang, B.; Yu, J.; Wang, H.; Chen, Y.; Lu, X.; Wang, G.; Zhou, X. Realizing high thermoelectric performance in p-type CaZn2Sb2-alloyed Mg3Sb2-based materials via band and point defect engineering. *Chem. Eng. J.* **2023**, *475*, 145988.

(22) Liu, R.; Chen, H.; Zhao, K.; Qin, Y.; Jiang, B.; Zhang, T.; Sha, G.; Shi, X.; Uher, C.; Zhang, W.; Chen, L. Entropy as a Gene-Like Performance Indicator Promoting Thermoelectric Materials. *Adv. Mater.* **2017**, *29*, 1702712.

(23) Liu, K.-J.; Zhang, Z.-W.; Chen, C.; Wei, L.-H.; He, H.-L.; Mao, J.; Zhang, Q. Entropy engineering in CaZn2Sb2−YbMg2Sb2 Zintl alloys for enhanced thermoelectric performance. *Rare Met.* **2022**, *41*, 2998−3004.

(24) Song, J.; Song, H. Y.; Wang, Z.; Lee, S.; Hwang, J.-Y.; Lee, S. Y.; Lee, J.; Kim, D.; Lee, K. H.; Kim, Y.; Oh, S. H.; Kim, S. W. Creation of two-dimensional layered Zintl phase by dimensional manipulation of crystal structure. *Sci. Adv.* **2019**, *5*, No. eaax0390.

(25) Liu, Q.; Liu, X.-C.; Zhang, J.; Liu, K.-F.; Xia, S.-Q. Enhanced Thermoelectric Performance of LiZnSb-Alloyed CaZn0.4Ag0.2Sb by Band Engineering. *ACS Appl. Mater. Interfaces* **2021**, *13*, 17809−17816.

(26) Balvanz, A.; Qu, J.; Baranets, S.; Ertekin, E.; Gorai, P.; Bobev, S. New n-Type Zintl Phases for Thermoelectrics: Discovery, Structural Characterization, and Band Engineering of the Compounds A2CdP2 (A = Sr, Ba, Eu). *Chem. Mater.* **2020**, *32*, 10697−10707.

(27) Kresse, G.; Hafner, J. Ab initio molecular dynamics for liquid metals. *Phys. Rev. B* **1993**, *47*, 558−561.

(28) Kresse, G.; Furthmüller, J. Efficient iterative schemes for ab initio total-energy calculations using a plane-wave basis set. *Phys. Rev. B* **1996**, *54*, 11169−11186.

(29) Perdew, J. P.; Ruzsinszky, A.; Csonka, G. I.; Vydrov, O. A.; Scuseria, G. E.; Constantin, L. A.; Zhou, X.; Burke, K. Restoring the Density-Gradient Expansion for Exchange in Solids and Surfaces. *Phys. Rev. Lett.* **2008**, *100*, 136406.

(30) Tran, F.; Blaha, P. Accurate Band Gaps of Semiconductors and Insulators with a Semilocal Exchange-Correlation Potential. *Phys. Rev. Lett.* **2009**, *102*, 226401.

(31) Heyd, J.; Scuseria, G. E.; Ernzerhof, M. Hybrid functionals based on a screened Coulomb potential. *J. Chem. Phys.* **2003**, *118*, 8207−8215.

(32) Ganose, A. M.; Park, J.; Faghaninia, A.; Woods-Robinson, R.; Persson, K. A.; Jain, A. Efficient calculation of carrier scattering rates from first principles. *Nat. Commun.* **2021**, *12*, 2222.

(33) Bardeen, J.; Shockley, W. Deformation Potentials and Mobilities in Non-Polar Crystals. *Phys. Rev.* **1950**, *80*, 72−80.

(34) Savelsberg, G. On Ternary Pnictides and Chalkogenides of Alkaline Metals and IB-resp. II B-Elements. *Z. Naturforsch., B* **1978**, *33*, 370−373.
(35) Toriyama, M. Y.; Carranco, A. N.; Snyder, G. J.; Gorai, P. Material descriptors for thermoelectric performance of narrow-gap semiconductors and semimetals. *Mater. Horiz.* **2023**, *10*, 4256−4269.
(36) Soni, A.; Yanyuan, Z.; Ligen, Y.; Aik, M. K. K.; Dresselhaus, M. S.; Xiong, Q. Enhanced Thermoelectric Properties of Solution Grown Bi2Te3−xSex Nanoplatelet Composites. *Nano Lett.* **2012**, *12*, 1203−1209.
(37) Devender; Gehring, P.; Gaul, A.; Hoyer, A.; Vaklinova, K.; Mehta, R. J.; Burghard, M.; Borca-Tasciuc, T.; Singh, D. J.; Kern, K.; Ramanath, G. Harnessing Topological Band Effects in Bismuth Telluride Selenide for Large Enhancements in Thermoelectric Properties through Isovalent Doping. *Adv. Mater.* **2016**, *28*, 6436−6441.
(38) Liu, S.; Peng, N.; Zhou, C.; Bai, Y.; Tang, S.; Ma, D.; Ma, F.; Xu, K. Fabrication of Bi2Te3-xSex nanowires with tunable chemical compositions and enhanced thermoelectric properties. *Nanotechnology* **2017**, *28*, 085601.
(39) Perdew, J. P.; Levy, M. Physical Content of the Exact Kohn-Sham Orbital Energies: Band Gaps and Derivative Discontinuities. *Phys. Rev. Lett.* **1983**, *51*, 1884−1887.
(40) Krukau, A. V.; Vydrov, O. A.; Izmaylov, A. F.; Scuseria, G. E. Influence of the exchange screening parameter on the performance of screened hybrid functionals. *J. Chem. Phys.* **2006**, *125*, 224106.
(41) Madsen, G. K. H.; Carrete, J.; Verstraete, M. J. BoltzTraP2, a program for interpolating band structures and calculating semi-classical transport coefficients. *Comput. Phys. Commun.* **2018**, *231*, 140−145.
(42) Sun, F.; Hong, A. Re-understanding of the deformation potential constant in the single crystal silicon. *Mater. Today Commun.* **2024**, *38*, 108316.
(43) Wei, S.-H.; Zunger, A. Predicted band-gap pressure coefficients of all diamond and zinc-blende semiconductors: Chemical trends. *Phys. Rev. B* **1999**, *60*, 5404−5411.
(44) Franceschetti, A.; Wei, S.-H.; Zunger, A. Absolute deformation potentials of Al, Si, and NaCl. *Phys. Rev. B* **1994**, *50*, 17797−17801.
(45) Quintela, C. X.; Rodríguez-González, B.; Rivadulla, F. Thermoelectric properties of heavy-element doped CrN. *Appl. Phys. Lett.* **2014**, *104*, 022103.
(46) Jood, P.; Mehta, R. J.; Zhang, Y.; Borca-Tasciuc, T.; Dou, S. X.; Singh, D. J.; Ramanath, G. Heavy element doping for enhancing thermoelectric properties of nanostructured zinc oxide. *RSC Adv.* **2014**, *4*, 6363.

https://doi.org/10.1021/acsaem.5c01933
ACS Appl. Energy Mater. 2025, 8, 11741−11748